Capillarity

Vol. 10, No. 1, p. 22-28, 2024

Short communication

CO_2 capillary trapping in layered sandstone dominated by inertial force and gravity

Yingwen Li, Yongfei Yang*, Mingzhe Dong

School of Petroleum Engineering, China University of Petroleum (East China), Qingdao 266580, P. R. China

Keywords:
Gravity segregation
CO_2 capillary trapping
layered heterogeneity
pore scale

Cited as:
Li, Y., Yang, Y., Dong, M. CO_2 capillary trapping in layered sandstone dominated by inertial force and gravity. Capillarity, 2024, 10(1): 22-28.
https://doi.org/10.46690/capi.2024.01.03

Abstract:
Capillary trapping is an important strategy to prevent CO_2 from escaping. Meanwhile, under immiscible conditions, CO_2 may travel upwards by gravity. Studying the long-term effects of gravity and layered heterogeneity on CO_2 transport is crucial for ensuring CO_2 storage security in aquifers. In this work, fluid flow experiments driven by inertial force and gravity are conducted in a specially constructed layered sandstone. Whether driven by inertial force or gravity, the variation in CO_2 distribution in the high-permeability layer is consistently the most significant factor. In the low-permeability layer, the saturation and capillary pressure distribution of CO_2 clusters vary less and the geometric shapes are also more complex, thus the CO_2 capillary trapping in this layer is more stable. This work demonstrates that the low-permeability layer can effectively prevent CO_2 from escaping upwards when the permeability ratio between layers approaches two.

1. Introduction

CO_2 storage is generally studied in two types of underground formations: aquifers and depleted oil and gas reservoirs (Alhosani et al., 2020, 2021; Song et al., 2023). When CO_2 migrates underground, it may be trapped by water or oil in the rock pores, a process called capillary trapping (Zhang et al., 2019; Zhou et al., 2019; Li et al., 2022; Xu et al., 2022). Andrew et al. (2013) imaged the pore-scale distribution of CO_2 clusters and confirmed that residual trapping can help ensure the safe storage of carbonate aquifers. Scanziani et al. (2018) imaged rocks containing water, oil and CO_2, and explained the CO_2 trapping mechanism in three-phase flow. In subsequent studies, Scanziani et al. (2020) further described the double capillary trapping phenomena that lead to high residual gas saturation. Moreover, Li et al. (2023) imaged the distribution of oil, CO_2 and water in artificial sandstones made of glass beads and quartz sand, and studied the influence of pore geometry on CO_2 capillary trapping. The above studies investigated the pore scale characteristics of CO_2 capillary trapping based on homogeneous porous media; however, rock heterogeneity is also an important factor impacting capillary trapping. Therefore, some scholars studied CO_2 plume migration at larger scales (such as meter-long cores) (Debbabi et al., 2017; Xu et al., 2020; Moreno and Rabinovich, 2021; Seyyedi et al., 2022). The results indicated that heterogeneity is important in determining residual trapping volume, and that local heterogeneity can lead to the fixation of small CO_2 plumes (Al-Bayati et al., 2018).

In the above works, the effect of gravity on gas migration over a long period was not considered. To ensure the stability of CO_2 storage, an analysis of gas-water flow dominated by inertial force and gravity over a longer timescale is needed. In this study, pore-scale fluid distribution in a layered sandstone during CO_2 and water flooding is described, and changes of CO_2 distribution during no-injection period is specifically analyzed. Compared to core-scale imaging, pore-scale imaging can finely characterize the obscure changes in fluid distribution and microscopic fluid geometry (Alhosani et al., 2019, 2021; Liu et al., 2022). Based on 10 sets of micro-CT images, the fluid saturation, capillary pressure distributions and CO_2

*Corresponding author.
E-mail address: b20020034@s.upc.edu.cn (Y. Li); yangyongfei@upc.edu.cn (Y. Yang); mingzhe.dong@ucalgary.ca (M. Dong).

Yandy Scientific Press

Received October 2, 2023; revised November 21, 2023; accepted November 13, 2023; available online November 16, 2023.

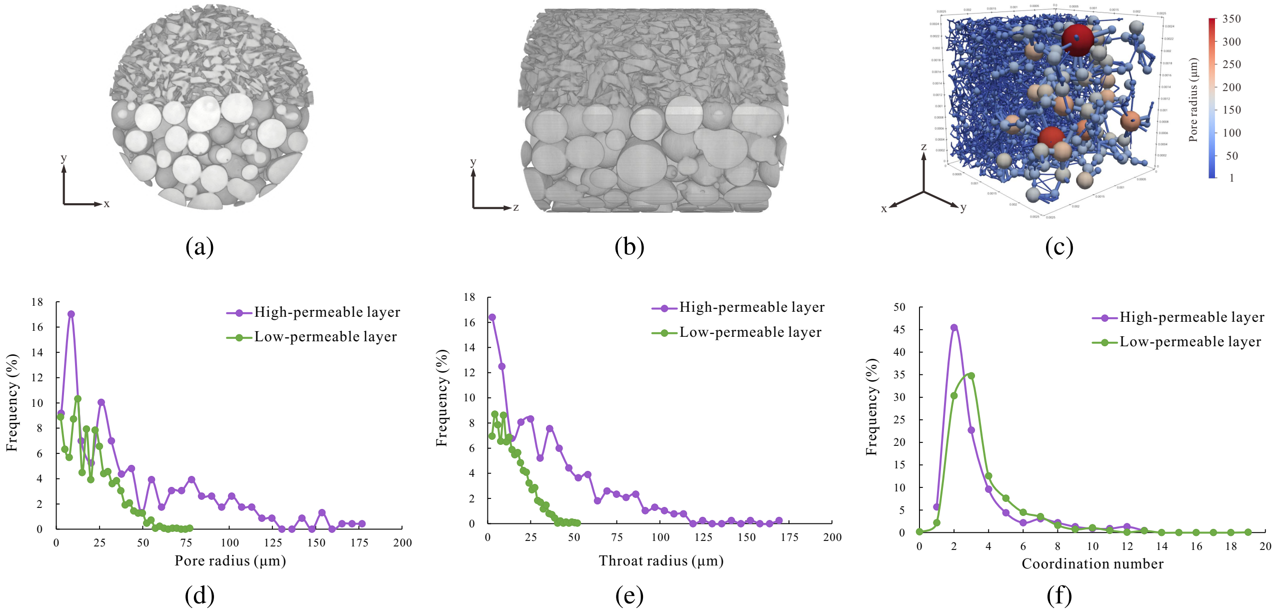

Fig. 1. (a) (b) 3D visualizations (800 × 800 × 800 voxel size) of the layered porous media at 4.51 μm voxel resolution, (c) pore network model of the layered porous media, (d) pore radius distributions, (e) throat radius distributions, and (f) coordination number distributions of the high and low-permeability layers, respectively.

Table 1. Petrophysical properties of the high- and low-permeability layers.

Type of layer	Average pore radius (μm)	Average throat radius (μm)	Coordination number
High-permeability	43.95	34.12	3.28
Low-permeability	20.17	14.57	3.50

cluster surface area-volume relationship are calculated to accurately characterize the migration of CO_2 in high- and low-permeability layers.

2. Methodology

2.1 Materials

The experiment is performed using an artificial layered core, with a diameter of 5 mm and length of 20 mm, drilled from a larger core. The high-permeability layer is composed of glass beads with an average diameter of 0.425 mm, while the low-permeability layer is composed of quartz sand with an average diameter of 0.178 mm. After obtaining the digital core of the dry core (Figs. 1(a) and 1(b)), a pore network model is extracted (Fig. 1(c)) and the relevant pore structure parameters are shown in Figs. 1(d) and 1(e) and 1(f). The porosities were determined with a Helium porosimeter to be 31.2% of the high-permeability layer and 30.1% of the low-permeability layer. Thus, the porosities of the high- and low-permeability layers are similar. However, the liquid permeability of the high-permeability layer (7.98 D) is almost twice as high as that of the low-permeability layer (4.01 D). The pore structure characteristics of the core are listed in Table 1. Water and CO_2 are the two fluids used in the displacement experiment. A small amount of KI is added to the water to better distinguish the two-phase fluid from the CT images. The physical properties of the fluid are shown in Table 2.

2.2 Flooding experiment

As shown in Fig. 2, the experiment includes gas injection, water flooding, and no injection period. In the gas injection process, CO_2 is injected into the water saturated core at a flow rate of 0.01 mL/min, and the core is scanned separately at 10 PV and 20 PV CO_2 injection. Then, the core is placed horizontally (with the high-permeability layer located below the low-permeability layer) for 24 hrs, 48 hrs and 72 hrs with no flow, followed by separate scanning. During the water flooding process, water is injected into the core at a flow rate of 0.01 mL/min and the core is scanned separately when injecting 10 PV and 20 PV of water. Finally, the imaging of the no-injection period is performed again. All subsequent analyses are based on the obtained 10 sets of digital cores.

2.3 Image acquisition and processing

3D images are obtained using an Xradia MicroXCT-400 scanner. During the scanning process, the voltage and power of the X-ray source are adjusted to 100 kV and 8 W. The centroid of the core is found at 0.4 × objective and then the objective is switched to 4 × to acquire the digital core with a resolution of 4.51 μm. The actual physical size corresponding to the

Table 2. Thermophysical properties of water and gas under experimental conditions (20°C and atmospheric pressure).

Fluid	Composition	Density (kg/m^3)	Viscosity (mPa·s)	Interfacial tension (mN/m)
Water	H_2O + 3.5% KI	1, 010	1.00	73.70
Gas	CO_2	1.82	0.02	

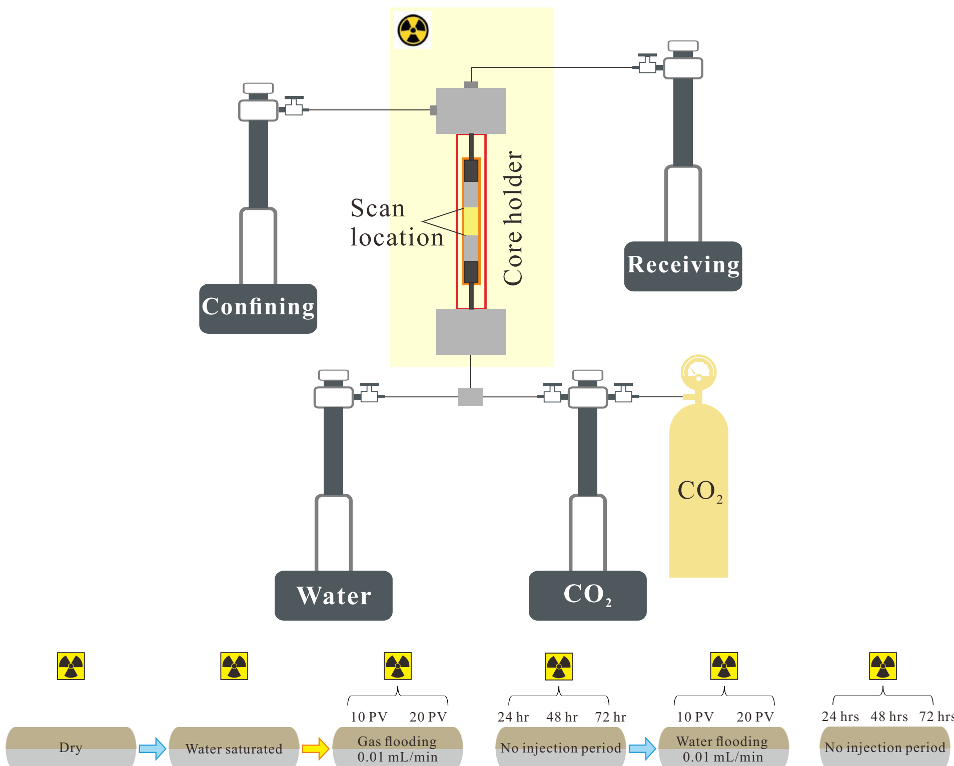

Fig. 2. The flow apparatus used to conduct drainage and imbibition experiments.

scanned area is 68.74 mm^3. All steps of image processing are performed by Avizo software, and the size of the extracted representative elementary volume is 920 × 920 × 923 voxels. The detailed image processing procedure is referred to Section 2.4 of the work by Yang et al. (2019).

3. Results and discussion

3.1 Distribution of CO_2

Although the porosities of high- and low-permeability layers are similar, there is significantly more CO_2 in the former after gas injection. CO_2 is distributed as large connected clusters in the pores of high-permeability layers and in the form of small bubbles in the pores of low-permeability layers (see Fig. 3, where each fluid cluster is labeled with a different color). After water flooding, the volume of CO_2 in the high-permeability layer is significantly decreased, while the distribution of CO_2 in the low-permeability layer remains almost unchanged. The CO_2 distributions in the layered core are consistent with the phenomenon reported for three-phase oil-water-gas systems (Li et al., 2023), and the complex pore geometry helps trap more residual CO_2. During the two no-injection periods, the spatial distribution of CO_2 continues to change (see the 2D slices). Especially in the high-permeability layer, the CO_2 movement phenomenon is more obvious. Since there is no other driving force, it can be assumed that gravity causes the CO_2 transport. On the contrary, lower CO_2 transport is observed in the low-permeability layer, which indicates that this layer to some extent prevents the upward transport of CO_2 under gravity. To further analyze the differences in CO_2 capillary trapping between high- and low-permeability layers, detailed quantitative characterizations of CO_2 clusters are conducted in the following sections.

3.2 CO_2 capillary-trapping capacity

Based on segmented images, the CO_2 saturation and capillary-trapping capacity (C_{trap}) of high- and low-permeability layers are calculated, where C_{trap} is equal to the saturation of CO_2 multiplied by porosity, which represents the amount of CO_2 securely stored per unit rock volume. It is found that CO_2 saturation increases during the no-injection period, with the change in saturation being more pronounced in the high-permeability layer. Moreover, during the no-injection period after water flooding, the CO_2 saturation of the high-permeability layer increases by 17.73%, while the CO_2 saturation of the low-permeability layer only increases

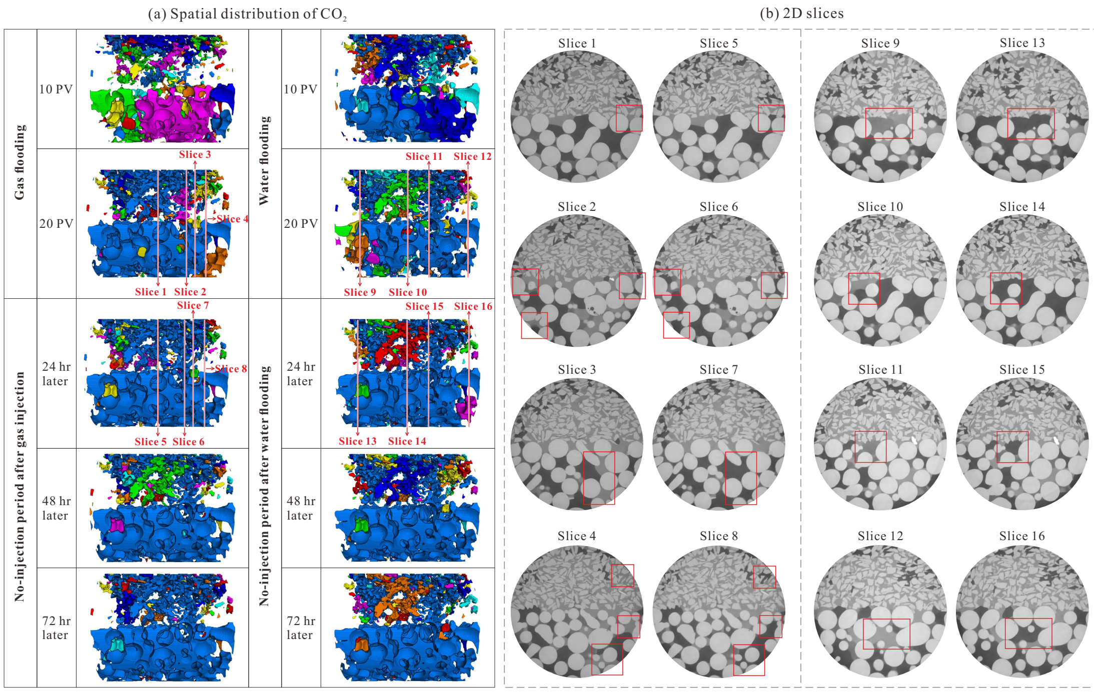

Fig. 3. Spatial distribution of CO_2 during gas injection, water flooding and two no-injection periods (a). The corresponding 2D slices are shown in (b). In the 2D slices, gas is black, water is dark gray, and particles are light gray. The red boxes show the migration of fluid caused by gravity during the no-injection period.

by 1.36%, indicating that the high-permeability layer is not conducive to the long-term stable storage of CO_2 (see Table 3). As observed in the CT images, the CO_2 saturation of the low-permeability layer changes less throughout the entire displacement process and no-injection period, indicating that the distribution of CO_2 in the low-permeability layer is relatively stable and this layer effectively prevents the CO_2 migration caused by gravity.

3.3 CO_2 capillary pressure distribution

After obtaining the curvature (C) of CO_2 clusters by image processing, the capillary pressure (p_c) of CO_2 clusters can be calculated ($p_c = \sigma_{gw}C$), with the positive and negative sign of capillary pressure indicating the direction. Table 4 shows the capillary pressure distribution of CO_2 clusters. The calculation results indicate that the range of capillary pressure distribution in the low-permeability layer is always higher than that in the high-permeability layer. Subsequent to water flooding, the capillary pressure of CO_2 clusters increases, which is caused by the segmentation of large connected CO_2 clusters into small clusters. It is found that the capillary pressure of CO_2 gradually decreases during the no-injection period, thus some of the small bubbles may converge into large bubbles during this time. Furthermore, the capillary pressure distribution range in the high-permeability layer varies greatly during the no-injection period, whereas that of the low-permeability layer varies less, suggesting that CO_2 capillary trapping in the low-permeability layer is more stable.

3.4 Relationship between CO_2 volume and surface area

The surface area-volume relationship of CO_2 clusters is another morphological descriptor of CO_2 clusters, which determines the remobilization and mass transfer of CO_2. A smaller surface area to volume ratio represents fluid clusters with more regular shapes, which are easier to mobilize. The volume V (μm^3) and surface area A (μm^2) of each CO_2 bubble during the displacements and no injection period are measured on the segmented images. The surface area-volume relationships can be well fitted by the power law correlation $A \sim V_p$ (related coefficient $R^2 > 0.99$), and the average value of these power law exponent p is about 0.77 (Fig. 4 and Table 5). This is basically consistent with the range of p-values (0.75 to 0.83) measured by Geistlinger et al. (2015) and Iglauer et al. (2016). After water flooding, the power index p increases, indicating a rise in S/V and a more complex morphology of residual CO_2 clusters after water flooding. The power exponent p of the low-permeability layer is greater than or equal to that of the high-permeability layer, indicating that the shapes of CO_2 clusters in the low-permeability layer are more complex and such fluid clusters are less likely to be mobilized. In addition, during the no-injection period, the power exponent p slightly decreases, thus it is speculated that some small bubbles may converge into larger bubbles during this time.

4. Conclusion

In this work, micro-displacement experiments are conducted on a specially constructed layered heterogeneous sandstone, and the fluid distributions of gas injection, water flood-

Table 3. Variations in CO_2 saturation and C_{trap} in high- and low-permeability layers.

Displacement stage		High-permeability layer		Low-permeability layer	
		CO_2 saturation (%)	C_{trap} (%)	CO_2 saturation (%)	C_{trap} (%)
Gas injection	10 PV	53.79	13.79	31.14	7.45
	20 PV	72.90	18.68	28.17	6.74
No-injection period	24 hrs later	84.56	21.67	28.36	6.78
	48 hrs later	85.54	21.92	28.00	6.70
	72 hrs later	87.57	22.45	28.35	6.78
Water flooding	10 PV	80.23	20.56	28.78	6.88
	20 PV	64.55	16.54	27.49	6.57
No-injection period	24 hrs later	79.92	20.48	27.90	6.67
	48 hrs later	81.21	20.81	27.90	6.67
	72 hrs later	82.28	21.09	28.85	6.90

Table 4. Capillary pressure distributions of CO_2 clusters in high- and low-permeability layers.

Displacement stage		Capillary pressure (kPa)	
		High-permeability layer	Low-permeability layer
Gas injection	10 PV	-286.30～129.83	-234.43～251.65
	20 PV	-284.26 124.25	-225.40 251.84
No-injection period	24 hrs later	-261.57～131.50	-225.05～235.87
	48 hrs later	-206.77～185.42	-225.80～233.94
	72 hrs later	-199.50～125.89	-225.20～231.84
Water flooding	10 PV	-241.70～129.30	-318.11～242.95
	20 PV	-341.70～207.02	-381.46～224.74
No-injection period	24 hrs later	-268.67～217.14	-376.13～228.83
	48 hrs later	-268.87～196.45	-377.75～213.77
	72 hrs later	-267.50～195.64	-376.54～210.70

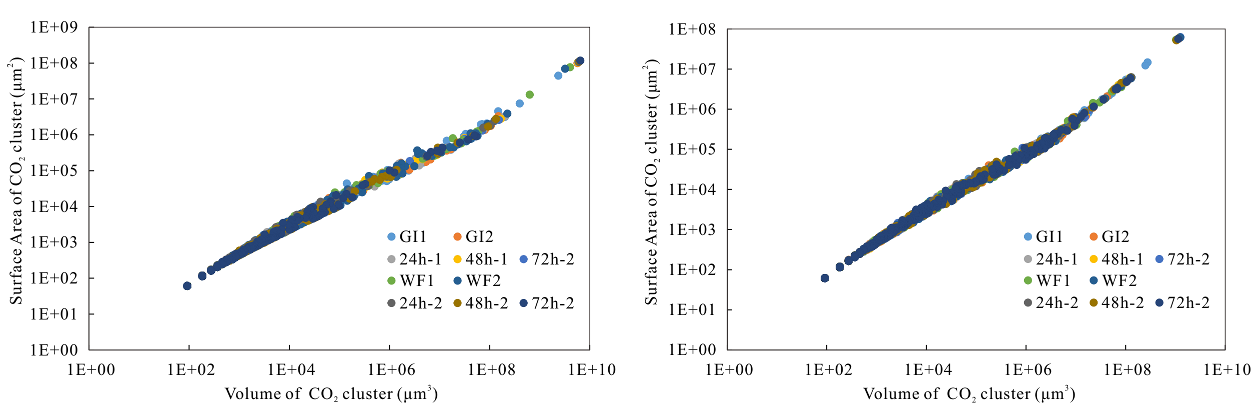

(a) (b)

Fig. 4. Surface area versus cluster volume for each CO_2 cluster in the high-permeability layer (a) and low-permeability layer (b).

Table 5. Capillary pressure distributions of CO_2 clusters in high- and low-permeability layers.

Displacement stage		Exponent p	
		High-permeability layer	Low-permeability layer
Gas injection	10 PV	0.769	0.776
	20 PV	0.758	0.769
No-injection period	24 hrs later	0.757	0.770
	48 hrs later	0.756	0.769
	72 hrs later	0.755	0.768
Water flooding	10 PV	0.770	0.772
	20 PV	0.769	0.773
No-injection period	24 hrs later	0.767	0.770
	48 hrs later	0.766	0.769
	72 hrs later	0.765	0.769

ing and no injection period are visualized. The effects of layered heterogeneity, inertial force and gravity on gas migration, CO_2 saturation spatial distribution and final trapping are also quantified. It is found that in the absence of inertial forces, the spatial distribution of fluids continues to change under the effect of gravity, especially in the high-permeability layer where CO_2 saturation changes more significantly. Meanwhile, there is less migration of CO_2 in the low-permeability layer and the change in saturation is smaller. The distribution of capillary pressure and the surface area-volume relationship of CO_2 clusters show that the shapes of CO_2 clusters in the low-permeability layer are more complex and these fluid clusters are less likely to be mobilized. Moreover, the range of capillary pressure distribution in the low-permeability layer is relatively small, indicating that CO_2 capillary trapping in this layer is more stable, effectively preventing gravity-induced CO_2 from escaping.

Acknowledgements

We would like to express our appreciation for the following financial support: National Key Research and Development Program of China (No. 2022YFE0203400), National Natural Science Foundation of China (Nos. 52034010 and 52288101).

Conflict of interest

The authors declare no competing interest.

References

Al-Bayati, D., Saeedi, A., Xie, Q., et al. Influence of permeability heterogeneity on miscible CO_2 flooding efficiency in sandstone reservoirs: An experimental investigation. Transport in Porous Media, 2018, 125(2): 341-356.

Alhosani, A., Lin, Q., Scanziani, A., et al. Pore-scale characterization of carbon dioxide storage at immiscible and near-miscible conditions in altered-wettability reservoir rocks. International Journal of Greenhouse Gas Control, 2021, 105: 103232.

Alhosani, A., Scanziani, A., Lin, Q., et al. In situ pore-scale analysis of oil recovery during three-phase near-miscible CO_2 injection in a water-wet carbonate rock. Advances in Water Resources, 2019, 134: 103432.

Alhosani, A., Scanziani, A., Lin, Q., et al. Pore-scale mechanisms of CO_2 storage in oilfields. Scientific reports, 2020, 10(1): 8534.

Andrew, M., Bijeljic, B., Blunt, M. J. Pore-scale imaging of geological carbon dioxide storage under in situ conditions. Geophysical Research Letters, 2013, 40(15): 3915-3918.

Debbabi, Y., Jackson, M. D., Hampson, G. J., et al. Capillary heterogeneity trapping and crossflow in layered porous media. Transport in Porous Media, 2017, 120(1): 183-206.

Geistlinger, H., Ataei-Dadavi, I., Mohammadian, S., et al. The impact of pore structure and surface roughness on capillary trapping for 2-D and 3-D porous media: Comparison with percolation theory. Water Resources Research, 2015, 51(11): 9094-9111.

Iglauer, S., Rahman, T., Sarmadivaleh, M., et al. Influence of wettability on residual gas trapping and enhanced oil recovery in three-phase flow: A pore-scale analysis by use of microcomputed tomography. SPE Journal, 2016, 21(6): 1916-1929.

Li, Y., Yang, Y., Dong, M., et al. Effect of pore structure and capillary number on gas-water flow patterns in carbonate rocks. SPE Journal, 2022, 27(4): 1895-1904.

Li, Y., Yang, Y., Dong, M., et al. In-situ imaging of CO_2 trapping and oil recovery in three-phase systems: Dependence on pore geometry and wettability. SPE Journal, 2023, 28(2): 768-782.

Liu, J., Tang, Q., Kou, J., et al. A quantitative study on the approximation error and speed-up of the multi-scale MCMC (Monte carlo markov chain) method for molecular dynamics. Journal of Computational Physics, 2022, 469: 111491.

Moreno, Z., Rabinovich, A. Impact of sub-core-scale heterogeneity on meter-scale flow and brine displacement in drainage by CO_2. Water Resources Research, 2021, 57(1): e2020WR028332.

Scanziani, A., Singh, K., Bultreys, T., et al. In situ characterization of immiscible three-phase flow at the pore scale for a water-wet carbonate rock. Advances in Water Resources, 2018, 121: 446-455.

Scanziani, A., Singh, K., Menke, H., et al. Dynamics of enhanced gas trapping applied to CO_2 storage in the presence of oil using synchrotron X-ray micro tomography. Applied Energy, 2020, 259: 114136.

Seyyedi, M., Clennell, M. B., Jackson, S. J. Time-lapse imaging of flow instability and rock heterogeneity impacts on CO_2 plume migration in meter long sandstone cores. Advances in Water Resources, 2022, 164: 104216.

Song, W., Prodanović, M., Yao, J., et al. Nano-scale wetting film impact on multiphase transport properties in porous media. Transport in Porous Media, 2023, 149(1): 5-33.

Xu, L., Myers, M., Li, Q., et al. Migration and storage characteristics of supercritical CO_2 in anisotropic sandstones with clay interlayers based on X-CT experiments. Journal of Hydrology, 2020, 580: 124239.

Xu, T., Tian, H., Zhu, H., et al. China actively promotes CO_2 capture, utilization and storage research to achieve carbon peak and carbon neutrality. Advances in Geo-Energy Research, 2022, 6(1): 1-3.

Yang, Y., Li, Y., Yao, J., et al. Formation damage evaluation of a sandstone reservoir via pore-scale X-ray computed tomography analysis. Journal of Petroleum Science and Engineering, 2019, 183: 106356.

Zhang, L., Wang, Y., Miao, X., et al. Geochemistry in geologic CO_2 utilization and storage: A brief review. Advances in Geo-Energy Research, 2019, 3(3): 304-313.

Zhou, J., Hu, N., Xian, X., et al. Supercritical CO_2 fracking for enhanced shale gas recovery and CO_2 sequestration: Results, status and future challenges. Advances in Geo-Energy Research, 2019, 3(2): 207-224.